A new substrate triggers susceptibility by uncoupling a bacterial multidrug resistance efflux pump

Peyton J. Spreacker[1‡], Nathan E. Thomas[1,3‡], Will F. Beeninga[1,4], Merissa Brousseau[1], Kylie M. Hibbs[1], Katherine A. Henzler-Wildman[1,2*]

[1]Department of Biochemistry, University of Wisconsin-Madison, Madison, WI 53703 USA

[2]Nuclear Magnetic Resonance Facility at Madison, University of Wisconsin-Madison, Madison WI 53703, USA

[3]*Current Address:* Department of Chemistry and Biochemistry, University of California-San Diego, La Jolla, CA, 92093

[4]*Current Address*: Mayo Medical Laboratories, Rochester, MN

[‡]Equal contribution authors

[*]Correspondence: henzlerwildm@wisc.edu

Abstract

Small multidrug resistance (SMR) transporters perform coupled antiport of protons and toxic substrates, contributing to antibiotic resistance through efflux of these compounds from the bacterial cytoplasm. Extensive biophysical studies of the molecular transport mechanism of the E. coli SMR transporter EmrE indicate that it should also be capable of performing proton/drug symport or uniport, either of which will lead to drug susceptibility rather than drug resistance in vivo. Here we show that EmrE does indeed confer susceptibility to some small molecule substrates in the native E. coli in addition to conferring resistance to known polyaromatic cation substrates. In vitro experiments show that substrate binding at a secondary site triggers uncoupled proton uniport that leads to susceptibility. These results suggest that the SMR transporters provide one avenue for bacterial-selective dissipation of the proton-motive force. This has potential for antibiotic development and disruption of antibiotic resistance due to drug efflux more broadly.

Introduction

There is an urgent need to better understand the underlying mechanisms of antibiotic resistance, including resistance due to drug efflux. The small multidrug resistance (SMR) transporters are found throughout the bacterial kingdom and efflux toxic compounds through coupled antiport of substrate and protons as illustrated in Figure 1[1–4]. The most widely studied member of this family, EmrE confers resistance to a broad array of toxic polyaromatic cations in *E. coli*[5,6]. Due to its small size, EmrE was proposed to be an ideal model for studying the minimal structural and mechanistic requirements for multidrug recognition and proton-coupled transport. However, this small transporter has proven to have surprisingly complex transport activity and mechanism[7–9].

Transporters have traditionally been classified as antiporters, uniporters, or symporters. Thus, the discovery that EmrE could perform coupled 2 H^+: 1 substrate (drug) antiport of a wide range of polyaromatic cations[10] to drive efflux defined its function for many years. Pure-exchange models of proton-coupled antiport focus on the key states and transitions needed for stoichiometric coupled antiport and assume that other states and transitions (leak pathways) contribute minimally to net transport. Recently, careful exploration of the states and transitions of EmrE using NMR revealed that this assumption was not valid for EmrE[9]. Expanding the mechanistic model to include all the states and transitions observed by NMR leads to a more complex free exchange model where proton/drug symport, proton uniport, and drug uniport are all theoretically possible in addition to the well-established proton/substrate antiport activity of EmrE (Fig. 1). The biological implications of these alternative transport pathways are significant – while H^+-driven antiport results in toxin efflux and a resistance phenotype *in vivo*, all the alternative pathways (symport or uniport) would result in toxin influx or PMF rundown, and thus should lead to a *susceptibility* phenotype in bacteria.

There is precedence for mutagenesis readily converting SMR transporter activity from conferring resistance to susceptibility *in vivo*[11]. The W63G-EmrE point mutant confers resistance to the clinical antibiotic erythromycin, but *susceptibility* to polyamine compounds[12], confirming that both transport phenotypes are possible for a single transporter. Of more potential clinical relevance is whether it is possible to shift *wild-type* (WT) EmrE from its well-established resistance activity to alternative transport modes that would confer susceptibility (Fig. 1). There are a few examples of WT transporters utilizing different transport modes to optimize physiological outcomes for sugar uptake under changing external conditions[13,14] or by preventing loss of acquired metals through back transport[15,16]. EmrE would represent a fundamentally different case where different modes of transport result in *opposite* biological outcomes of resistance versus susceptibility to toxic compounds.

Finding a way to favor these deleterious transport modes may present a new strategy to combat antibiotic resistance. For known drug substrates, 2H+:1drug antiport is kinetically favored under physiological conditions[17], but substrate identity can alter the rate of key steps in EmrE's transport cycle over three orders of magnitude[18,19]. Rate changes of this magnitude have the potential to bias flux through alternative transport pathways and shift the balance of net transport[9].

Here we experimentally test whether substrate identity can switch the transport phenotype in WT EmrE. Using an unbiased small molecule phenotypic screen, we identify new substrates to which EmrE confers resistance *and* new substrates to which it confers susceptibility. For one of the strongest susceptibility substrates, harmane, we use a combination of *in vitro* and *in vivo* assays to

determine the transport mechanism underlying the novel phenotype. This work opens the possibility that alternative transport pathways of multidrug transporter represent a novel target for antibiotic development.

Results

Unbiased screen reveals new substrates

Previous EmrE substrate screens have focused on quaternary ammonium compounds (QACs) and quaternary cationic compounds (QCCs) commonly transported by multidrug efflux pumps[5,10,20,21]. To better explore the substrate profile of EmrE, we performed an unbiased screen using the Phenotypic Microarray assay from Biolog, Inc. This screen assesses the impact of diverse compounds on *E. coli* metabolic output in a differential comparison of MG1655Δ*emrE E. coli* expressing either wildtype or non-functional EmrE (E14Q-EmrE). If metabolic output was greater when wildtype EmrE was expressed, it indicates that functional EmrE is beneficial, and the compound was classified as a resistance hit. If metabolic output was greater when E14Q-EmrE was expressed, it indicates that functional EmrE is detrimental and the compound was classified as a susceptibility hit (Fig. 2, Extended Data Fig. 1, Extended Data Table 1, see methods for selection criteria). As shown in Fig. 2a, the screen identified compounds in both categories, resistance or susceptibility.

The well-established EmrE substrate methyl viologen (MV^{2+}) was the strongest resistance hit with the highest possible score according to our criteria (+8). Acriflavine, another known substrate, was also a strong +4 resistance hit, confirming that the Biolog assay accurately reports on EmrE drug resistance phenotypes. Chelerythrine chloride has not been previously identified as an EmrE substrate but showed a strong +5 resistance phenotype. Microplate growth assays of *E. coli* expressing either wildtype or E14Q-EmrE in the presence of MV^{2+} or chelerythrine chloride confirmed the resistance phenotype (Fig. 2c,d). Chelerythrine chloride has been used as an antibacterial agent for drug-resistant infections[22], so EmrE-conferred resistance may be clinically relevant.

EmrE's resistance activity has been well characterized in *E. coli*, but a susceptibility phenotype for WT EmrE has not previously been reported. The top three susceptibility hits identified in the Biolog screen were: harmane (-6), hexachlorophene (-6), and 18-crown-6-ether (-5). Compared to the other susceptibility hits, hexachlorophene is extremely insoluble therefore it was not evaluated further. In microplate growth assays, E14Q-EmrE cells grew normally in the presence of 18-crown-6-ether (Fig. 2e, red line) or harmane (Fig. 2f, red line), but cells expressing WT EmrE had growth deficiencies after three to five hours of treatment (black lines). This confirmed that functional EmrE confers *susceptibility* rather than resistance to these compounds.

Harmane susceptibility is due to proton leak

EmrE-mediated drug resistance phenotypes can only be explained by the canonical proton/drug antiport mechanism, but drug susceptibility can arise from three potential transport mechanisms: drug uniport, proton uniport, or proton/drug symport (Fig. 1). To better understand how EmrE confers susceptibility to harmane, we turned to a solid supported membrane electrophysiology (SSME) assay recently developed in our lab to characterize the ion-coupling behavior of secondary active transporters (Extended Data Figure 3)[23,24]. SSME allows the detection of net charge movement in proteoliposomes adsorbed onto a gold electrode sensor upon buffer perfusion and is ideal for measuring small transport currents produced by moderate-flux transporters such as EmrE[25].

The hallmark of coupled transport is the ability of downhill transport of one substrate to drive uphill transport of another substrate. In the assay design shown in Fig. 3a, this will result in reversal of the direction of net charge movement in distinct and predictable ways for symport or antiport (Extended Data Figure 3). The difference between antiport and symport is simply which orientation of the drug gradient (relative to the smaller proton gradient) enhances proton-driven transport and which orientation reverses net transport. In the case of drug- or proton-uniport, net transport depends solely on the gradient and net charge of the uniported substrate, either drug or proton.

We first measured net charge movement under the three gradient conditions depicted in Fig. 3a for transport of $MeTPP^+$, which is known to be antiported by EmrE (Fig. 3b,c; Extended Data Figure 4a,b). Proteoliposomes reconstituted with E14Q-EmrE were used as negative controls and produced minimal signals under all conditions, regardless of substrate. In the absence of drug, the proton gradient alone induces a small positive current in WT EmrE proteoliposomes, indicating minimal proton leak. When $MeTPP^+$ is added, we observe transport reversal as expected for 2 H^+ / 1 $MeTPP^+$ antiport.

In contrast, net transport does not reverse when harmane is the substrate (Fig. 3d,e; Extended Data Figure 4c,d). Instead, the net charge transport is constant and positive (down the proton gradient), under all conditions. This lack of reversal between inwardly- and outwardly-directed drug gradients is indicative of uncoupled proton transport (leak). This proton leak is triggered by harmane, since the signal is larger with harmane than the background proton leak in the absence of drug. To confirm this, we co-varied the internal and external harmane concentration to maintain zero harmane gradient while using a 2-fold proton gradient to drive transport. The hyperbolic dependence of peak current on the harmane concentration indicates a saturable, direct binding interaction between harmane and EmrE that triggers proton uniport (Fig. 3f; Extended Data Figure 4e,f).

Reexamining the cell growth assays indicates the harmane phenotype appears around the 5 hour mark (Fig. 2e,f), approximately the point at which fermentable sugars are consumed[26] and cells become more reliant on the PMF for ATP production when *E.coli* are grown in LB. Thus, both the *in vitro* and *in vivo* assays are consistent with harmane triggering an EmrE-mediated uncontrolled proton leak.

Different substrate interactions with EmrE

Harmane triggers fundamentally different transport behavior by EmrE compared to previously known substrates, both in liposomal transport assays and bacterial growth assays. This raises an important question: How does harmane interact with EmrE to elicit such an unexpected outcome? We used NMR chemical shift perturbations (CSPs) to explore whether harmane interacts with EmrE in a novel way. NMR chemical shifts are exquisitely sensitive to the surrounding environment, and CSPs reflect both binding and structural changes that alter the chemical environment of residues throughout the protein. For these experiments we used S64V-EmrE, a point mutant that suppresses the dynamics of EmrE (to give higher quality NMR spectra) without disrupting binding of TPP^+ or related substrates[27]. We first confirmed that this mutant also binds harmane with an affinity comparable to WT EmrE by intrinsic tryptophan fluorescence quenching analysis[18] (Fig. 3g). We then assessed the CSPs for EmrE binding of either TPP^+ or harmane to understand the very different functional behavior with each of these substrates.

Large CSPs are observed across S64V-EmrE upon TPP^+ binding to S64V-EmrE (Fig. 4a, Extended Data Fig. 5). CSPs near E14 confirm that TPP^+ interacts with the established primary binding site of EmrE. The broader CSP profile across more distal regions of EmrE is consistent with the consequent conformational change that ultimately leads to alternating access and TPP^+ transport across the membrane[9,19,28,29]. In contrast, the CSPs upon harmane binding are of much smaller magnitude (Fig. 4b; Extended Data Fig. 5). Although there are CSPs near E14 upon harmane binding, it is evident that harmane does not cause the same large-scale perturbations observed for TPP^+, and thus has a distinct mode of interaction with EmrE.

A secondary substrate binding site

Twenty years ago, ^{31}P solid-state NMR studies of TPP^+ binding to EmrE showed the presence of a second drug binding site in the loops between the TM helices[30]. Those experiments suggested that TPP^+ bound first to this peripheral low-affinity site before binding to the high-affinity site defined by E14. To probe whether harmane might interact with this putative ill-defined secondary site, we

repeated the NMR CSP studies of harmane and TPP^+ binding with E14Q-EmrE (Fig. 4c,d, Extended Data Fig. 6). With the well-established primary drug binding site abolished [8,31,32] any CSPs observed upon drug addition must be due to interactions with secondary binding sites in EmrE. Indeed, small but statistically significant CSPs are observed for both TPP^+ (Fig. 4c) and harmane (Fig. 4d) binding E14Q-EmrE. Unlike WT-EmrE, where harmane and TPP^+ have very different CSP profiles, the magnitude and pattern of CSPs is comparable for either substrate binding to E14Q-EmrE, with CSPs located in the C-terminal tail, the C-terminal half of TM2, and the TM3-TM4 loop. Due to the antiparallel topology of the EmrE homodimer, the 2-3 loop and C-terminal tail of one protomer are near the 3-4 loop from the other protomer. TM2 has been shown to be involved in substrate specificity[5], and the loops and tail have previously been suggested to be involved in a secondary binding site and participate in drug- and proton-binding[30,33,34]. These results are consistent with a putative secondary binding site in this region of EmrE. While TPP^+ also interacts with this peripheral site (Fig. 4c), TPP^+ interactions with the primary binding site are much stronger (Fig. 4a)[30,35], such that interactions with the peripheral site are only apparent when the primary E14 binding site is removed by mutation. This suggests not only that both drugs can interact with EmrE in the absence of the primary binding site E14, but that the mode of this secondary interaction is potentially similar.

The NMR data suggests a potential mechanism of action for harmane-induced proton leak (Fig. 4e,f). A recent investigation of coupling between EmrE's C-terminal residue H110 and the central binding site E14 led us to propose that proton transport by EmrE is gated by the C-terminal tail in the absence of drug[34]. Drug binding to a secondary site in the loops, originally suggested by drug-monitored ^{31}P NMR[30], could unlock this gate, allowing access to the primary binding site at E14 and transport to proceed as depicted in the E14-centered model of Figure 1. In the case of TPP^+, the drug moves from the peripheral low-affinity site to the high-affinity binding site at E14 (Fig. 4e) once the secondary gate is open, leading to coupled transport with the most common $2H^+$:$1TPP^+$ antiport pathway highlighted in orange in Figure 1. In the case of harmane, the drug remains in the peripheral site (Fig. 4f) but the open gate allows proton access to E14 and alternating access results in proton leak as highlighted in red in Figure 1. The ability of harmane to trigger uncontrolled proton leak as the dominant transport mode cannot be explained by models that only permit coupled antiport and seek to minimize or exclude leak pathways[7,18]. A gated model also explains why proton release from EmrE occurs at the same rate as drug binding, despite the very different affinities and on-rates[18]. This result provides additional experimental evidence justifying more complex models for EmrE transport as previously proposed[9,18].

Discussion

Our prior NMR studies had suggested that it would be possible for EmrE to carry out drug uniport, proton uniport, and even proton-coupled drug symport in addition to its well-characterized proton-coupled drug antiport activity[9,17], and that it might be possible to bias EmrE toward different transport pathways by switching the small molecule substrate[9,19]. The data presented here shows that it is indeed the case, not just *in vitro*, but *in vivo*. These results have two important implications: First, we demonstrate that small molecules can modulate transporter activity to the extent that the biological outcome is effectively reversed. To date, efforts to target multidrug resistance due to efflux have primarily focused on developing inhibitors of clinically relevant efflux pumps[36]. The results presented suggests that it may be possible to go beyond simply blocking transport and instead develop molecules that switch transport mode so that these multidrug resistance transporters instead confer susceptibility. Second, we demonstrate that small molecules can trigger proton-mediated proton leak and proton-motive-force rundown to a level detrimental to cell growth and survival. SMR transporters are found throughout the bacterial kingdom but not in other organisms[37–39], so targeting them would provide bacterial selectivity and a potential avenue for dissipation of the proton motive force in a more selective way than general membrane active agents. Targeting bacterial bioenergetics as an alternative to cell envelope biogenesis or macromolecular biosynthesis is an area of active interest for novel antibiotic development[40–43] as well as synergy or collateral susceptibility with current antibiotics[44–47]. Moreover, since a majority of bacterial drug efflux pumps are proton-coupled[48], dissipation of the PMF may inhibit drug resistance due to efflux more broadly.

Kinetic studies of purified transporters show that some transporters appear to be tightly coupled and highly efficient, while others are more loosely coupled. The experimental challenges of performing these experiments have limited the number of transporters whose mechanism has been rigorously characterized. More recently, there has been renewed interest in kinetic modeling to understand how these more complex network models still achieve relatively efficient coupled transport and may be important for optimizing overall biological function[17,49,50]. In ATP-coupled transport systems, more significant “leak” (uncoupled ATP hydrolysis) is observed for promiscuous transporters than for highly selective transporters. For example, the multidrug efflux pump P-glycoprotein exhibits significant levels of basal ATP hydrolysis[51]. Loose coupling between the driving force, whether that consists of an electrochemical ion gradient or ATP hydrolysis, and substrate transport may be a requirement of multidrug recognition and efflux, as tight binding generally requires highly specific and selective interactions between the protein and the substrate. The possibility that loose coupling would extend to ion-coupled multidrug transporters, including the SMR family, was originally discussed more than 20 years ago[52]. Here we show that it is possible for a small molecule

to exploit this property of promiscuous multidrug transporters and trigger protein-mediated proton-motive-force rundown. If loose coupling is required for multidrug efflux, targeting dissipative pathways in multidrug transporters may represent a new general strategy for combatting antibiotic resistance, either through development of novel proton-motive-force-dissipating antibiotics or in combination to restore efficacy of current antibiotics.

Acknowledgements:

We thank Trey Sato for his assistance in using the OmniLog Instrument for Biolog Assays with funding from the Great Lakes Bioenergy Research Center under U.S. Department of Energy, Office of Science, Office of Biological and Environmental Research Award Number DE-SC0018409. This study made use of the National Magnetic Resonance Facility at Madison, which is supported by NIH grant P41GM103399 (NIGMS) and R24GM141526 (NIGMS). Research reported in this publication was supported by NIH grant R01GM095839 and R35GM141748.

Author Contributions:

PJS conceptualized the assays, generated methods, analyzed data, validated results, created figures, supervised experiments, wrote the original draft, and edited the manuscript. NET conceptualized the assays, generated methods, analyzed data, validated results, created figures, wrote the original draft, and edited the manuscript. WFB generated methods, performed experiments, and edited the manuscript. MB generated methods, performed experiments, analyzed data, validated results, generated figures, and edited the manuscript. KMH performed experiments and edited the manuscript. KAHW conceptualized the assays, analyzed data, validated results, supervised the research, wrote the original draft, generated figures, edited the manuscript and acquired funding for the work.

Declaration of interest: The authors declare no competing interests.

Data Availability: All solution NMR assignments can be found at the BMRB (https://bmrb.io/) using the following accession numbers: S64V-EmrE, drug free (51024), S64V-EmrE, harmane bound (51025), S64V-EmrE, TPP^+ bound (51026), E14Q-EmrE, drug free (51027), E14Q-EmrE, harmane bound (51031), and E14Q-EmrE, TPP^+ bound (51030). Biolog data was deposited at MendeleyData at the following link: https://data.mendeley.com/datasets/tpcdgw7h6m/draft?a=d615d927-f94d-4858-a6af-196b089b4fb3.

References:

1. Brown, M. H. & Skurray, R. A. Staphylococcal multidrug efflux protein QacA. *J Mol Microbiol Biotechnol* **3**, 163–170 (2001).
2. Pérez-Varela, M., Corral, J., Aranda, J. & Barbé, J. Roles of Efflux Pumps from Different Superfamilies in the Surface-Associated Motility and Virulence of Acinetobacter baumannii ATCC 17978. *Antimicrob Agents Chemother* **63**, e02190-18 (2019).
3. Srinivasan, V. B. & Rajamohan, G. KpnEF, a new member of the Klebsiella pneumoniae cell envelope stress response regulon, is an SMR-type efflux pump involved in broad-spectrum antimicrobial resistance. *Antimicrob Agents Chemother* **57**, 4449–4462 (2013).
4. Willsey, G. G. *et al.* Pulmonary Surfactant Promotes Virulence Gene Expression and Biofilm Formation in Klebsiella pneumoniae. *Infect Immun* **86**, e00135-18 (2018).
5. Saleh, M., Bay, D. C. & Turner, R. J. Few Conserved Amino Acids in the Small Multidrug Resistance Transporter EmrE Influence Drug Polyselectivity. *Antimicrob Agents Chemother* **62**, e00461-18 (2018).
6. Schuldiner, S. EmrE, a model for studying evolution and mechanism of ion-coupled transporters. *Biochim Biophys Acta* **1794**, 748–762 (2009).
7. Li, J., Her, A. S. & Traaseth, N. J. Asymmetric protonation of glutamate residues drives a preferred transport pathway in EmrE. *PNAS* **118**, (2021).
8. Morrison, E. A., Robinson, A. E., Liu, Y. & Henzler-Wildman, K. A. Asymmetric protonation of EmrE. *J Gen Physiol* **146**, 445–461 (2015).
9. Robinson, A. E., Thomas, N. E., Morrison, E. A., Balthazor, B. M. & Henzler-Wildman, K. A. New free-exchange model of EmrE transport. *Proc Natl Acad Sci U S A* **114**, E10083–E10091 (2017).
10. Rotem, D. & Schuldiner, S. EmrE, a multidrug transporter from Escherichia coli, transports monovalent and divalent substrates with the same stoichiometry. *J Biol Chem* **279**, 48787–48793 (2004).
11. Son, M. S. *et al.* Mutagenesis of SugE, a small multidrug resistance protein. *Biochem Biophys Res Commun* **312**, 914–921 (2003).
12. Brill, S., Falk, O. S. & Schuldiner, S. Transforming a drug/H+ antiporter into a polyamine importer by a single mutation. *Proc Natl Acad Sci U S A* **109**, 16894–16899 (2012).
13. Bazzone, A., Zabadne, A. J., Salisowski, A., Madej, M. G. & Fendler, K. A Loose Relationship: Incomplete H+/Sugar Coupling in the MFS Sugar Transporter GlcP. *Biophys J* **113**, 2736–2749 (2017).
14. Henderson, R. & Poolman, B. Proton-solute coupling mechanism of the maltose transporter from Saccharomyces cerevisiae. *Sci Rep* **7**, 14375 (2017).
15. Bozzi, A. T. *et al.* Structures in multiple conformations reveal distinct transition metal and proton pathways in an Nramp transporter. *eLife* **8**, e41124 (2019).
16. Bozzi, A. T., Bane, L. B., Zimanyi, C. M. & Gaudet, R. Unique structural features in an Nramp metal transporter impart substrate-specific proton cotransport and a kinetic bias to favor import. *J Gen Physiol* **151**, 1413–1429 (2019).
17. Hussey, G. A., Thomas, N. E. & Henzler-Wildman, K. A. Highly coupled transport can be achieved in free-exchange transport models. *J Gen Physiol* **152**, (2019).
18. Adam, Y., Tayer, N., Rotem, D., Schreiber, G. & Schuldiner, S. The fast release of sticky protons: kinetics of substrate binding and proton release in a multidrug transporter. *Proc Natl Acad Sci U S A* **104**, 17989–17994 (2007).
19. Morrison, E. A. & Henzler-Wildman, K. A. Transported substrate determines exchange rate in the multidrug resistance transporter EmrE. *J Biol Chem* **289**, 6825–6836 (2014).
20. Bay, D. C. & Turner, R. J. Small multidrug resistance protein EmrE reduces host pH and osmotic tolerance to metabolic quaternary cation osmoprotectants. *J Bacteriol* **194**, 5941–5948 (2012).

21. Bay, D. C., Stremick, C. A., Slipski, C. J. & Turner, R. J. Secondary multidrug efflux pump mutants alter Escherichia coli biofilm growth in the presence of cationic antimicrobial compounds. *Res Microbiol* **168**, 208–221 (2017).
22. Zhang, X. *et al.* Chelerythrine Chloride: A Potential Rumen Microbial Urease Inhibitor Screened by Targeting UreG. *Int J Mol Sci* **22**, 8212 (2021).
23. Shcherbakov, A. A. *et al.* Structure and dynamics of the drug-bound bacterial transporter EmrE in lipid bilayers. *Nat Commun* **12**, 172 (2021).
24. Thomas, N. E., Feng, W. & Henzler-Wildman, K. A. A Solid Supported Membrane Electrophysiology Assay for Efficient Characterization of Ion-Coupled Transport. *J Biol Chem* 101220 (2021) doi:10.1016/j.jbc.2021.101220.
25. Bazzone, A., Barthmes, M. & Fendler, K. SSM-Based Electrophysiology for Transporter Research. *Methods Enzymol* **594**, 31–83 (2017).
26. Baev, M. V., Baev, D., Radek, A. J. & Campbell, J. W. Growth of Escherichia coli MG1655 on LB medium: monitoring utilization of sugars, alcohols, and organic acids with transcriptional microarrays. *Appl Microbiol Biotechnol* **71**, 310–316 (2006).
27. Wu, C. *et al.* Identification of an Alternating-Access Dynamics Mutant of EmrE with Impaired Transport. *J Mol Biol* **431**, 2777–2789 (2019).
28. Cho, M.-K., Gayen, A., Banigan, J. R., Leninger, M. & Traaseth, N. J. Intrinsic Conformational Plasticity of Native EmrE Provides a Pathway for Multidrug Resistance. *J. Am. Chem. Soc.* **136**, 8072–8080 (2014).
29. Gayen, A., Leninger, M. & Traaseth, N. J. Protonation of a glutamate residue modulates the dynamics of the drug transporter EmrE. *Nat Chem Biol* **12**, 141–145 (2016).
30. Glaubitz, C. *et al.* 31P-CP-MAS NMR studies on TPP^+ bound to the ion-coupled multidrug transport protein EmrE. *FEBS Lett* **480**, 127–131 (2000).
31. Muth, T. R. & Schuldiner, S. A membrane-embedded glutamate is required for ligand binding to the multidrug transporter EmrE. *EMBO J* **19**, 234–240 (2000).
32. Yerushalmi, H. & Schuldiner, S. An Essential Glutamyl Residue in EmrE, a Multidrug Antiporter from Escherichia coli *. *Journal of Biological Chemistry* **275**, 5264–5269 (2000).
33. Banigan, J. R., Gayen, A., Cho, M.-K. & Traaseth, N. J. A structured loop modulates coupling between the substrate-binding and dimerization domains in the multidrug resistance transporter EmrE. *J Biol Chem* **290**, 805–814 (2015).
34. Thomas, N. E. *et al.* The C terminus of the bacterial multidrug transporter EmrE couples drug binding to proton release. *J Biol Chem* **293**, 19137–19147 (2018).
35. Ong, Y. S., Lakatos, A., Becker-Baldus, J., Pos, K. M. & Glaubitz, C. Detecting Substrates Bound to the Secondary Multidrug Efflux Pump EmrE by DNP-Enhanced Solid-State NMR. *Journal of the American Chemical Society* **135**, 15754–15762 (2013).
36. Thakur, V., Uniyal, A. & Tiwari, V. A comprehensive review on pharmacology of efflux pumps and their inhibitors in antibiotic resistance. *European Journal of Pharmacology* **903**, 174151 (2021).
37. Bay, D. C. & Turner, R. J. Small Multidrug Resistance Efflux Pumps. in *Efflux-Mediated Antimicrobial Resistance in Bacteria: Mechanisms, Regulation and Clinical Implications* (eds. Li, X.-Z., Elkins, C. A. & Zgurskaya, H. I.) 45–71 (Springer International Publishing, 2016). doi:10.1007/978-3-319-39658-3_3.
38. Kermani, A. A., Macdonald, C. B., Gundepudi, R. & Stockbridge, R. B. Guanidinium export is the primal function of SMR family transporters. *Proc Natl Acad Sci U S A* **115**, 3060–3065 (2018).
39. Kolbusz, M. A., Slotboom, D. J. & Lolkema, J. S. Genomic distribution of the small multidrug resistance protein EmrE over 29 Escherichia coli strains reveals two forms of the protein. *FEBS J* **280**, 244–255 (2013).
40. Farha, M. A., Verschoor, C. P., Bowdish, D. & Brown, E. D. Collapsing the Proton Motive Force to Identify Synergistic Combinations against Staphylococcus aureus. *Chemistry & Biology* **20**, 1168–1178 (2013).

41. Hards, K. & Cook, G. M. Targeting bacterial energetics to produce new antimicrobials. *Drug Resist Updat* **36**, 1–12 (2018).
42. Hasenoehrl, E. J., Wiggins, T. J. & Berney, M. Bioenergetic Inhibitors: Antibiotic Efficacy and Mechanisms of Action in Mycobacterium tuberculosis. *Frontiers in Cellular and Infection Microbiology* **10**, 815 (2021).
43. Stokes, J. M. *et al.* A Deep Learning Approach to Antibiotic Discovery. *Cell* **180**, 688-702.e13 (2020).
44. Copp, J. N. *et al.* Mechanistic Understanding Enables the Rational Design of Salicylanilide Combination Therapies for Gram-Negative Infections. *mBio* **11**, e02068-20 (2020).
45. Feng, X. *et al.* Antiinfectives targeting enzymes and the proton motive force. *Proc Natl Acad Sci U S A* **112**, E7073-7082 (2015).
46. Lázár, V. *et al.* Bacterial evolution of antibiotic hypersensitivity. *Mol Syst Biol* **9**, 700 (2013).
47. Roemhild, R. & Andersson, D. I. Mechanisms and therapeutic potential of collateral sensitivity to antibiotics. *PLOS Pathogens* **17**, e1009172 (2021).
48. Henderson, P. J. F. *et al.* Physiological Functions of Bacterial 'Multidrug' Efflux Pumps. *Chem Rev* **121**, 5417–5478 (2021).
49. Bisignano, P. *et al.* A kinetic mechanism for enhanced selectivity of membrane transport. *PLoS Comput Biol* **16**, e1007789 (2020).
50. Burtscher, V., Schicker, K., Freissmuth, M. & Sandtner, W. Kinetic Models of Secondary Active Transporters. *Int J Mol Sci* **20**, E5365 (2019).
51. Sharom, F. J., Yu, X., Chu, J. W. & Doige, C. A. Characterization of the ATPase activity of P-glycoprotein from multidrug-resistant Chinese hamster ovary cells. *Biochem J* **308**, 381–390 (1995).
52. Krupka, R. M. Uncoupled Active Transport Mechanisms Accounting for Low Selectivity in Multidrug Carriers: P-Glycoprotein and SMR Antiporters. *Journal of Membrane Biology* **172**, 129–143 (1999).

METHODS

Plasmids and Strains

All *in vivo* experiments were performed in MG1655 Δ*emrE E. coli* cells transformed with a low copy number, leaky expression plasmid. Protein expression utilized BL21 (Gold) DE3 *E. coli* transformed with a pET15b plasmid containing the respective EmrE construct.

Biolog Phenotypic Microarrays

MG1655 Δ*emrE E. coli* cells expressing either WT- or E14Q-EmrE constructs were grown on LB-Amp media overnight at 37°C. The phenotype microarray tests followed the established protocols of standard phenotype microarray (PM) procedures for *E. coli* and other gram-negative bacteria (12). PM01-20 plates were used to screen both WT- and E14Q-EmrE expressing *E. coli* (http://www.biolog.com/products-static/phenotype_microbial_cells_overview.php). Overnight plates were resuspended in IF-0a inoculating fluid (Biolog) to an optical density of 0.37. The cells were diluted by a factor of 6 into IF-0a media plus Redox Dye A and 20mM glucose was added for PM3-8 plates. Cells were diluted to a 1:200 dilution in IF-10a media (Biolog) with Redox Dye A for PM9-20

plates. PM plates were inoculated with 100µL of cell suspensions per well. The microplates were incubated at 37°C and read using the OmniLog instrument every 15min for 24 h. The area under the resulting metabolic curves was determined for cells expressing WT-EmrE or E14Q-EmrE. The difference was calculated using the equation:

$$\Delta Area = Area_{WT} - Area_{E14Q} \quad \text{(Eq. 1)}$$

This equation resulted in positive values for greater respiration by cells expressing WT-EmrE and negative values for greater respiration by cells expressing non-functional EmrE. The 10% trimmed mean was then calculated for each data set (WT replicate 1, WT replicate 2, E14Q replicate 1, E14Q replicate 2) separately for each transporter as variation between replicates can arise due to minor deviations between plate sets or in the exact concentration of dye or OD of cells upon dilution on different days. The standard deviation was then calculated among known non-hits (selecting at least 50 wells out of the 960 total wells in a single data set) to determine the cut-off values for actual hits. Individual wells were assessed as hits if the calculated Delta value (equation 1) was more than two standard deviations from the 10% trimmed mean. For each hit, a value of +1 was assigned for resistance hits (positive Delta) and a value of -1 was assigned for susceptibility hits (negative Delta). These values were then summed across all eight wells for a single compound (4 wells of the same compound per plate set * 2 replicates, with a max score of ±8. Final resistance or susceptibility hits were assigned if the total score was ≥ +3 (resistance) or ≤ -3 (susceptibility). This definition was chosen since small total hit scores of ±1 or ±2 could arise by chance using the ± 2*SD cutoff to score individual wells. Values of ±3 recognize consistent hits across multiple replicates and/or different concentrations of the same compound. Our cutoff is not set higher since the 4 wells of each compound on a single plate set include different concentrations and some concentrations may not be sufficient to elicit a phenotype.

Microplate Growth Assays

Cells expressing plasmids of interest were grown in Mueller-Hinton broth (Sigma, 100µg/mL ampicillin, pH 7.0) from a single colony to an OD of 0.2 at 37 °C. The cells were then diluted to a final OD of 0.01 in 384-well microplates containing concentration ranges of MV^{2+}, harmane, 18-crown-6-ether, and chelerythrine chloride. The plates were incubated and shaken in a microplate reader (BMG-Labtech) at 37°C. OD_{600} was measured every 5 minutes for 20 hours. Experiments were performed with four biological replicates and data were analyzed using Igor Pro v8 (WaveMetrics Inc.).

IC_{50} assays

MG1655 Δ*emrE E. coli* cells expressing either WT or E14Q-EmrE were grown overnight at 37 °C from a single colony. Concentration ranges of ethidium bromide (0-5 mM) and harmane (0-0.4mM) were assayed in microplates with a starting OD_{600} of 0.1. Plates were then incubated with shaking for 18 hours with shaking at 37 °C. OD_{600} endpoints were taken using a BMG plate reader. Relative growth was calculated by dividing the measured OD_{600} from a given concentration by the OD_{600} for cells containing no drug. The data was performed in triplicate and fit to a simple sigmoid equation using Igor Pro v8 (WaveMetrics Inc.).

EmrE expression and purification

BL21 Gold (DE3) *E. coli* were transformed with pET15b-EmrE, pET15b-S64VEmrE, or pET15b-E14QEmrE plasmids and grown in M9 minimal media to an OD_{600} of 0.9. The bacteria were flash cooled and then induced with 0.33M IPTG overnight at 17 °C. The *E. coli* cells were collected with centrifugation, lysed, the membrane fraction solubilized with decylmaltoside (DM), and the proteins purified using NiNTA IMAC chromatography followed by size exclusion chromatography (SEC) on a Superdex 200 column as previously described[19]. Protein concentrations were determined using absorbance at 280 nm with an extinction coefficient of 38,400 L/mol cm[53].

Solid Supported Membrane Electrophysiology Transport Assays

WT- and E14Q-EmrE were expressed and purified, with the final SEC performed in assay buffer (50 mM MES, 50 mM MOPS, 50 mM bicine, 100 mM NaCl, 2 mM $MgCl_2$, 40 mM DM, pH 7). All buffers were carefully adjusted to the desired pH exclusively with NaOH to ensure consistent Cl^- concentrations across the membrane for transport assays. Protein was reconstituted into 1-palmitoyl-2-oleoyl-sn-glycero-3-phosphocholine (POPC) proteoliposomes at a lipid-to-protein ratio of 1:400 in pH 7 assay buffer. Briefly, 15 mg/ml stocks of POPC were diluted in assay buffer and incubated at 45 °C for 1 hour. Lipids were bath sonicated for 1 min then octyl glucoside (OG) was added to a final concentration of 0.5%. Lipids were sonicated for an additional 30 seconds and returned to 45 °C to incubated for 15 minutes. SEC fractions containing purified protein in DM were added to the lipid solution and incubated at RT for 25 minutes then detergent was removed with Amberlite XAD-2 as previously described [54]. As a negative control, POPC lipids were put through a simulated reconstitution process without protein. Amberlite was removed from each sample via gravity column and uniform liposomes were obtained by extrusion through a 0.2 µM membrane using an Avanti MiniExtruder. All SSME data was acquired using a Nanion SURFE2R N1 instrument. Liposome

aliquots were thawed, diluted 2-fold, and briefly sonicated. 10 µL of liposomes were used to prepare 3 mm sensors as previously described[24]. Prior to experiments, sensor capacitance and conductance values were obtained to ensure sensor quality. For all experiments, buffers contained 50 mM MES, 50 mM MOPS, 50 mM bicine, 100 mM NaCl, and 2 mM MgCl2 with internal pH values of 7.3 and external pH values of 7.0. For inward-facing drug gradients, external drug concentration was 8 µM and internal drug concentration was 0.5 µM. For outward-facing drug gradients, internal drug concentration was 8 µM and external drug concentration was 0.5 µM. Both internal and external drug concentration was 8 µM for the zero-gradient data. Sensors were rinsed with at least 500 µL of internal buffer prior to each measurement to set the internal buffer, pH, and drug concentrations as described in[24]. Data acquisition occurred in three stages. First, sensors were perfused with internal buffer, then transport was initiated by perfusion of the external buffer, and finally, perfusion of the internal buffer re-equilibrated the sensors. Signals were obtained by integrating the current during perfusion of the external buffer, with the final 100 ms of the initial internal buffer perfusion used as the baseline. Reported data are average values of at least three sensors, with error bars representing the standard error of the mean.

Intrinsic Tryptophan Assays

Purified WT- and S64V-EmrE were reconstituted into isotropic bicelles of DMPC/DPHC (q=0.33) as previously described[54]. Reconstitution of purified EmrE into liposomes was performed as described above for SSME transport assays but using DMPC lipids with an EmrE:DMPC ratio of 1:75. Bicelle stocks (2X) were prepared by dissolving DMPC in assay buffer containing 100 mM MOPS pH 7.0, 20 mM NaCl to a final concentration of 300 mM and incubating at 45 °C for 1.5 hrs. DHPC was then added to a final concentration of 100 mM to create q=0.33 isotropic bicelles, incubated an additional hour, and subjected to 3 freeze/thaw cycles. Harmane was prepared to a maximal concentration of 800 µM in assay buffer with 1X bicelle stock and rotated for 72 hours then serial diluted into black 96-well flat-bottom plates. WT- and S64V-EmrE in DMPC/DHPC bicelles were added to a final dimer concentration of 10 µM and the plate was incubated at room temperature for one hour. The final assay volume was 200 µL and each concentration was present in triplicate. Endpoint fluorescence was determined using a TECAN Spark and data analysis was performed in Igor Pro v8. Data were fit to a single binding isotherm detailed in the following equation:

$$F_{obs}=F_{EH}[EH]+F_{E}[E] \qquad \text{(Eq. 2)}$$

Where F_{obs} is the observed fluorescence, F_{EH} is the fluorescence of the EmrE functional dimer bound to harmane, [EH] is the concentration of EmrE functional dimer bound to harmane, F_E is the fluorescence of the EmrE functional dimer, and [E] is the concentration of EmrE functional dimer.

[EH] is calculated from the following equation:

$$[EH]=\frac{(E_T+H_{add}+K_d)-\sqrt{(E_T+H_{add}+K_d)^2-4E_TH_{add}}}{2} \qquad \text{(Eq.3)}$$

Where E_T is the total concentration of EmrE functional dimer in the sample, H_{add} is the total added harmane in the sample, and K_d is the dissociation constant.

The concentration of unbound EmrE functional dimer ([E]) is given by the following equation:

$$[E]=1-[EH] \qquad \text{(Eq.4)}$$

NMR assignments and chemical shift perturbations

S64V- and E14Q-EmrE were triple labeled using 1 g $^{15}NH_4Cl$, 0.75 g $^{2}H,^{13}C$-glucose, and 0.5 g CND-Isogro per liter of M9 minimal media. Purified WT- and S64V-EmrE were reconstituted into isotropic bicelles of DMPC/DPHC (q=0.33) following the protocol of[54] as described above for the intrinsic tryptophan assays but with an EmrE:DMPC ratio of 1:75. NMR data were collected on a 750MHz Avance III Bruker spectrometer at 45 °C using samples with 0.8-1 mM ^{2}H, ^{15}N, ^{13}C S64V- and E14Q-EmrE in DMPC/DHPC bicelles. For detailed buffer conditions, experimental details, and spectrometers, see BMRB depositions found in the STAR Methods Key Resources Table. Triple-resonance backbone walk experiments (TROSY-HNCA, TROSY HNcoCA, TROSY HNCO, and TROSY-HNcaCO, TROSY-HNCACB) were acquired for drug-free S64V-EmrE at pH 6.5, harmane-bound S64V-EmrE at pH 5.8, TPP^+-bound S64V-EmrE at pH 5.8 and drug-free E14Q-EmrE at pH 5.8. Amide assignments were transferred to other pH values using pH titrations, and from drug-free E14Q-EmrE to TPP^+- or harmane-bound E14Q-EmrE using substrate titrations.

Chemical shift perturbations between drug-free and drug-bound spectra were calculated as described in [19,27] using the following equation:

$$\Delta\omega_{tot}=\sqrt{(\Delta\omega_H)^2+(0.154\Delta\omega_N)^2} \qquad \text{(Eq. 5)}$$

With $\Delta\omega_{tot}$ representing the weighted average of the differences in amide proton ($\Delta\omega_H$) and nitrogen ($\Delta\omega_N$) chemical shifts.

Methods References

53. Morrison, E. A. *et al.* Antiparallel EmrE exports drugs by exchanging between asymmetric structures. *Nature* **481**, 45–50 (2011).

54. Morrison, E. A. & Henzler-Wildman, K. A. Reconstitution of integral membrane proteins into isotropic bicelles with improved sample stability and expanded lipid composition profile. *Biochimica et Biophysica Acta (BBA) - Biomembranes* **1818**, 814–820 (2012).

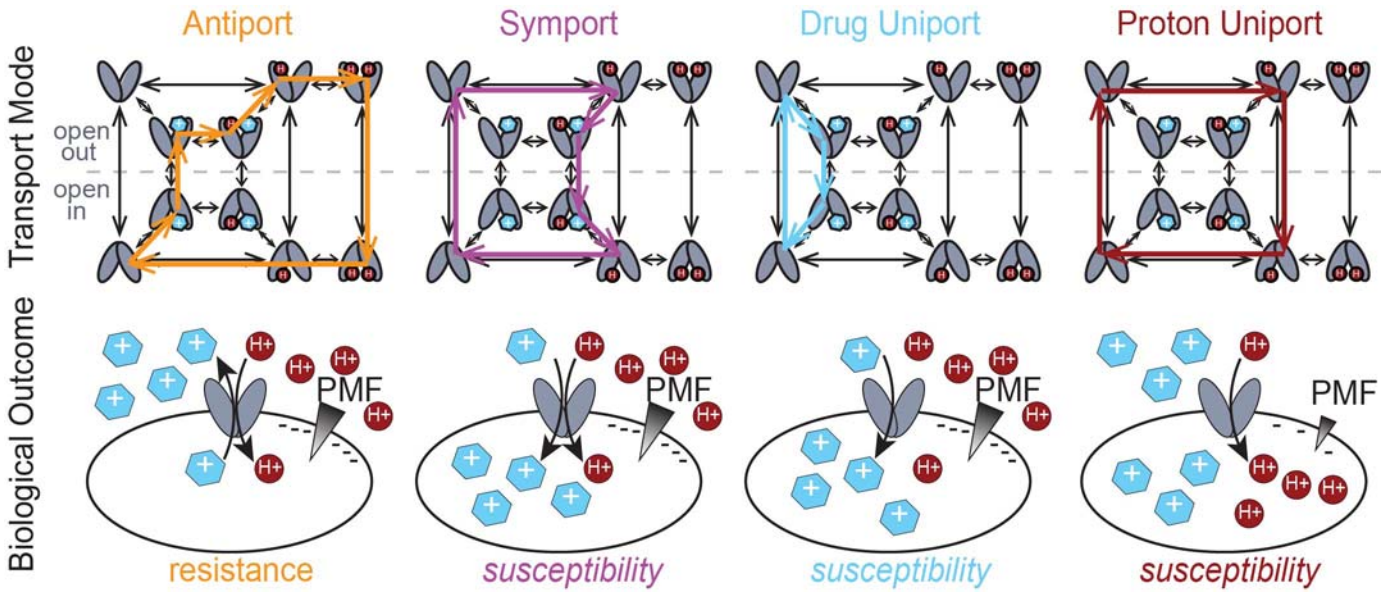

Figure 1: Different transport modes of EmrE result in different biological outcomes. The well-established coupled antiport of proton and drug (orange, top) by EmrE leads to drug resistance *in vivo* (orange, bottom). The Free Exchange Model suggests that EmrE should also be able to perform coupled symport (purple), drug uniport (blue), or proton uniport (maroon), any of which would lead susceptibility rather than resistance *in vivo*. The most likely pathway depends on the relative rates of the microscopic steps in the transport cycle, including drug on- and off-rates and the rate of alternating access between open-in and open-out conformations in each state (apo, proton-bound, drug-bound, etc.). Thus, different substrates can lead to different dominant modes of transport and opposing biological outcomes in cells.

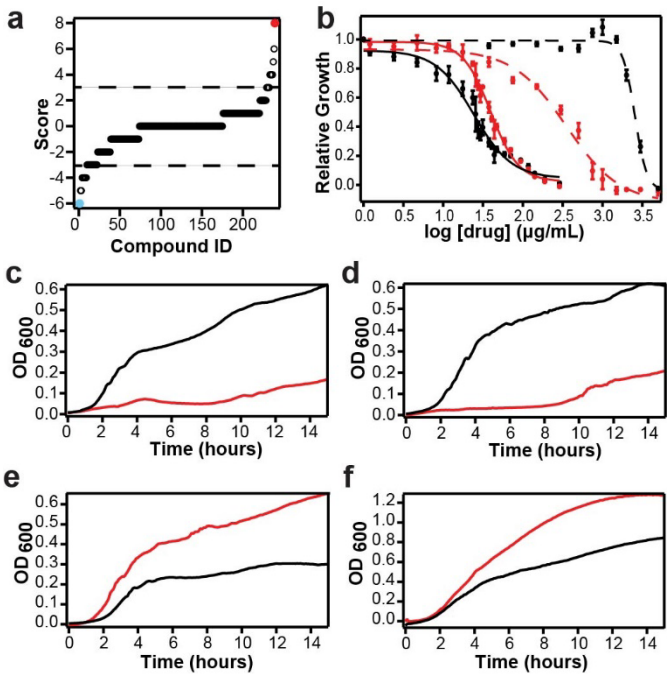

Figure 2: EmrE can confer either resistance or susceptibility *in vivo*. (a) Biolog phenotype microarray results sorted by hit score for all 240 compounds in the screen (see Methods). Scores above +3 or below -3 are considered resistance or susceptibility hits, respectively, based on differential between functional (WT) and non-functional (E14Q-EmrE). The strongest resistance hits (red) and susceptibility hits (cyan) were tested in growth assays (c-f). (b) IC_{50} curves of WT- (black) and E14Q-EmrE (red) are shown for ethidium bromide (dashed lines, resistance) and harmane (solid lines, susceptibility). Note that cells expressing WT-EmrE have a 40% lower IC_{50} value than cells expressing E14Q-EmrE in the presence of harmane. MG1655 ΔemrE *E. coli* expressing WT-EmrE (black) or E14Q-EmrE (red) were grown in the presence of (c) 0.5 mM methyl viologen (MV^{2+}), (d) 0.05 mM chelerythrine chloride (CC), (e) 0.1 mM 18-crown-6-ether, or (f) 0.13 mM harmane. As expected, *E. coli* expressing WT-EmrE grew better than *E. coli* expressing E14Q-EmrE in the presence of MV^{2+} and CC (c, d), consistent with a resistance phenotype. In contrast, *E. coli* expressing non-functional, E14Q-EmrE better than *E. coli* expressing WT-EmrE in the presence of 18-crown-6-ether and harmane, (e, f), consistent with a susceptibility phenotype.

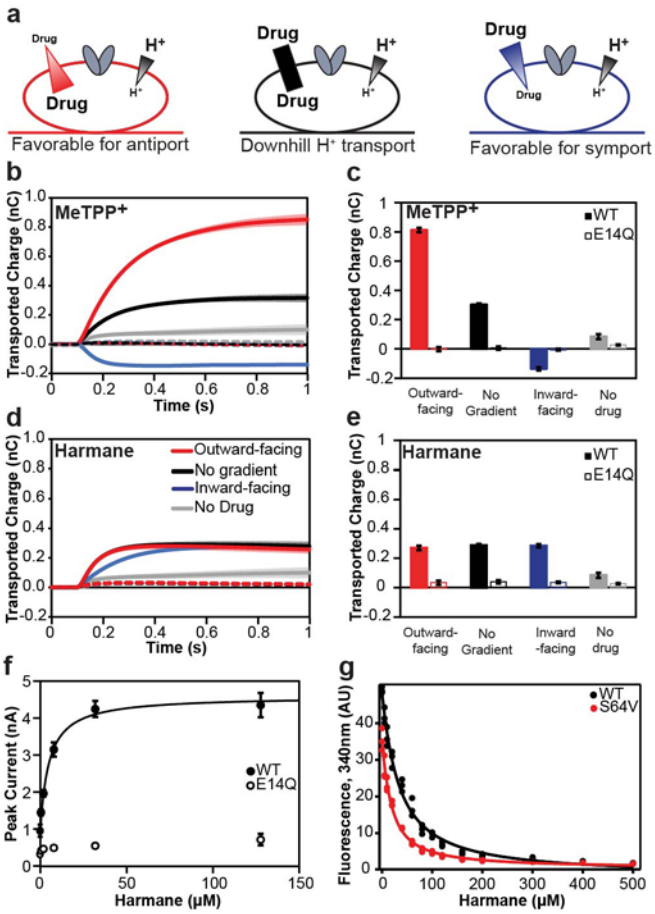

Figure 3: Harmane induces proton flux through EmrE. We used solid-supported membrane electrophysiology to experimentally verify the transport mode of $MeTPP^+$ and determine the transport mode of harmane *in vitro* (see Extended Data Figure 3 for expected outcomes for different transport modes). $MeTPP^+$ (a-b) behaves as expected for an antiported substrate. The total transported charge reverses when the drug gradient is inverted, characteristic of coupled antiport. In contrast, the harmane transport signal (c-d) is the same regardless of the harmane gradient, matching the expected behavior for downhill proton transport (proton leak). The current is minimal in the absence of drug (b, c; gray) or for liposomes containing non-functional E14Q-EmrE (dashed lines) in either case, indicating that the observed charge transport is due to substrate-triggered EmrE activity. (e) Peak current of downhill proton transport by EmrE recorded by SSME increases with harmane concentration and saturates, indicating the uncoupled proton transport is dependent on direct binding of harmane. The transport fits to Michaelis-Menten kinetics with a K_m value of 5 ± 1μM. (f) Harmane quenches intrinsic tryptophan fluorescence of both WT- (black) and S64V- (red) EmrE in a dose-dependent manner, with apparent K_d values of 29 ± 2μM and 14 ± 1μM respectively, confirming that harmane binds WT- and S64V-EmrE with similar affinity.

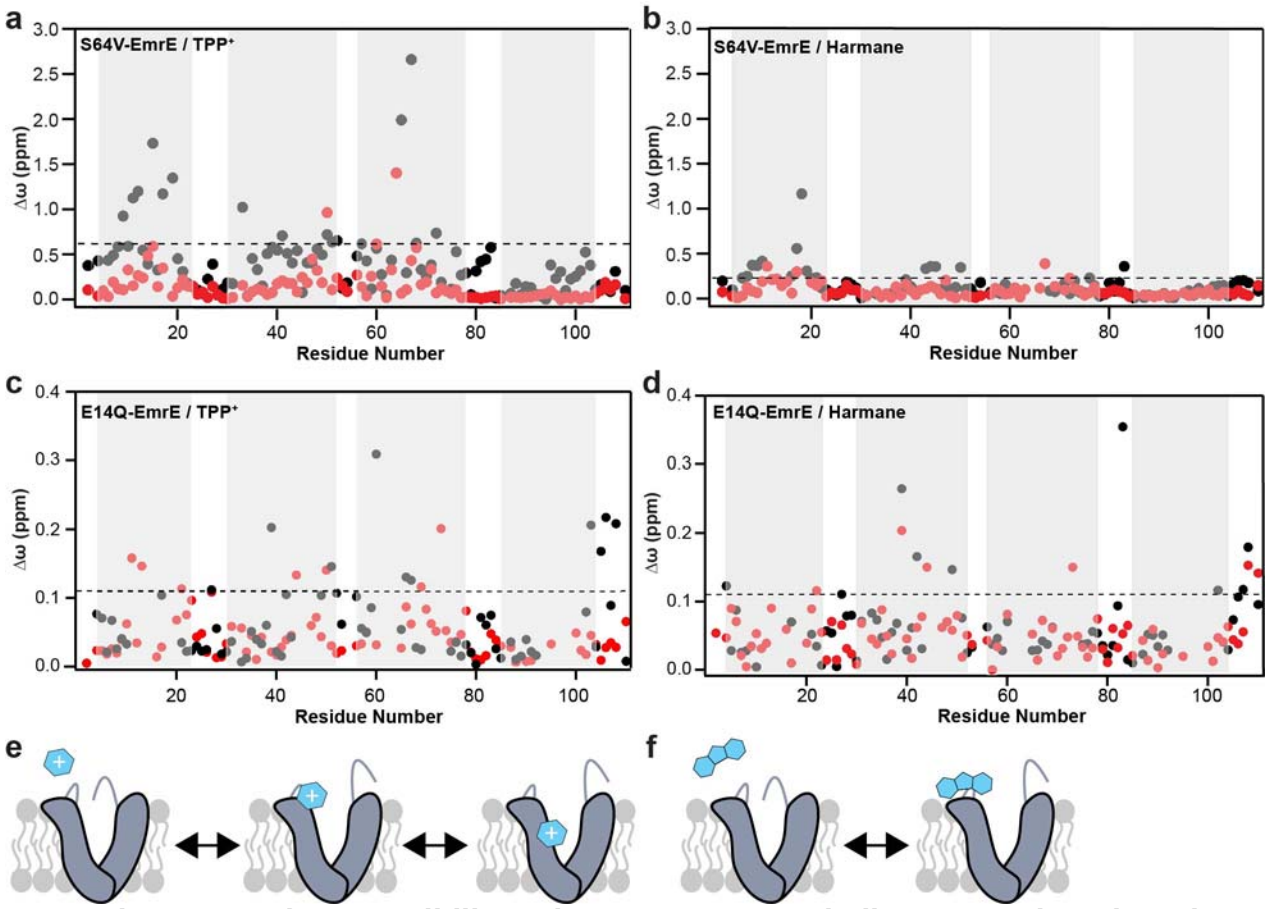

Figure 4: Resistance and susceptibility substrates prompt similar CSPs when the primary binding site is abolished. To understand how TPP^+ and harmane interact with EmrE, the backbone amide chemical shift perturbations of EmrE upon drug-binding ($\Delta\omega = \omega_{drug\ free} - \omega_{drug\ bound}$) was measured in isotropic bicelles using NMR. CSPs are shown for binding TPP^+ (a) or harmane (b) to functional EmrE (S64V-EmrE reduces protein dynamics without affecting substrate binding). Data is plotted for chain A (red) and chain B (black) as a function of residue number with the TM helices 1-4 indicated by the gray shading. Note that the magnitude of CSPs is much greater for TPP^+ binding than for harmane binding. E14Q-EmrE removes the glutamate residue that defines the primary binding site necessary for drug antiport *in vitro* and resistance *in vivo*. Repeating the CSP experiments with this mutant results CSPs with similar magnitude and location upon binding either TPP^+ (c) or harmane (d), confirming a secondary binding site for both substrates. Cartoon models show both TPP^+ (e) and harmane (f) bind the peripheral site and open the secondary gate, allowing E14-mediated transport pathways as shown in Figure 1. Only TPP+ moves into the primary binding site at E14 triggering coupled antiport, while harmane remains at the periphery and only protons bind E14 and are transported.

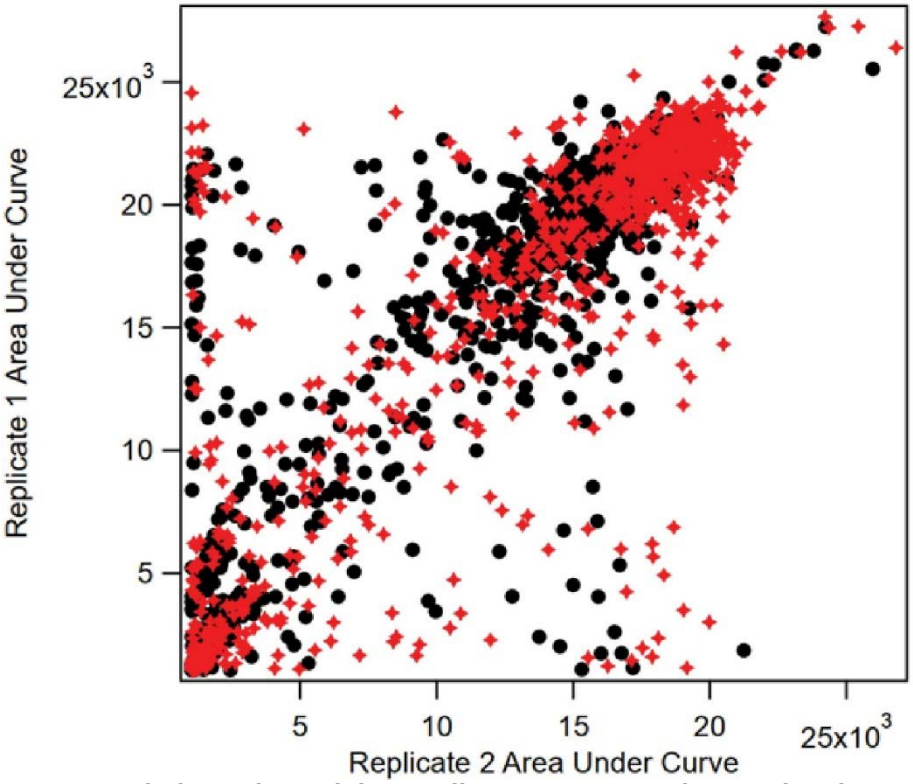

Extended Data Figure 1: Two independent Biolog replicates are strongly correlated. To quantify the correlation between replicates of the Biolog phenotype microarray, the area under the curve for all data in both biological replicates of the phenotype microarray for both WT-EmrE (black circles) and E14Q-EmrE (red diamonds) were plotted. The correlation constant for these data are 0.85 for WT and 0.84 for E14Q. These data were the basis for the hit threshold determination for results from EmrE data. Divergence in the data may stem from plate-to-plate differences in initial OD of cells, final compound concentration, and volume of sample.

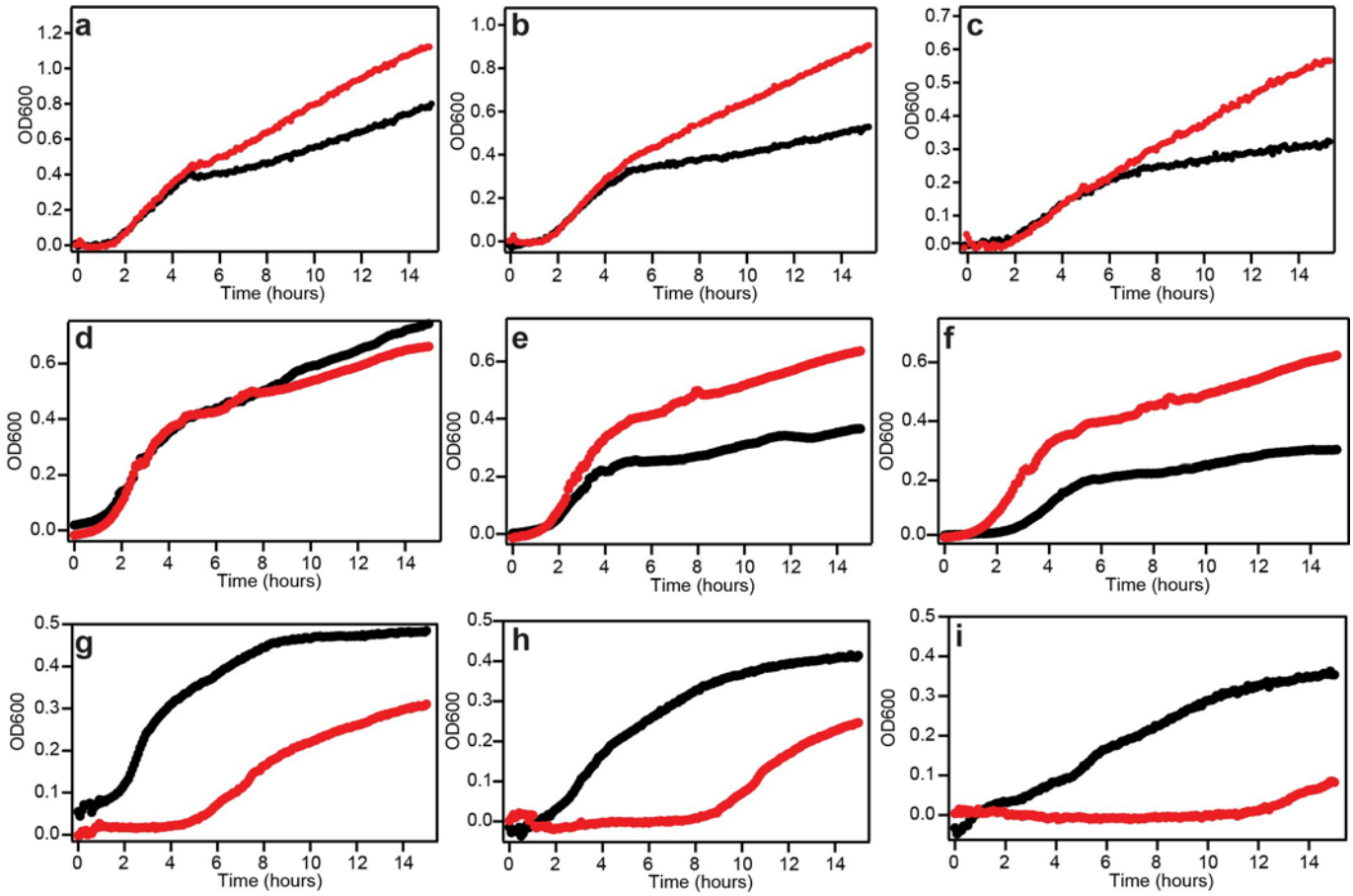

Extended Data Figure 2: Growth curve phenotypes are dose dependent. To further validate the results of the Biolog phenotype microarray, growth curves at varying concentrations of harmane (A, 0.0325 mM; B, 0.065 mM; and C, 0.13 mM), 18-crown-6-ether (D, 0.1 mM; E, 0.6 mM; and F, 3 mM), and chelerythrine chloride (G, 0.2 mM; H, 0.4 mM; and I, 0.8 mM) were performed. In all cases, the expected phenotypes (susceptibility for harmane and 18-crown-6-ether, and resistance for chelerythrine chloride) were observed with increasing compound concentration. The curves shown are an average of four biological replicates.

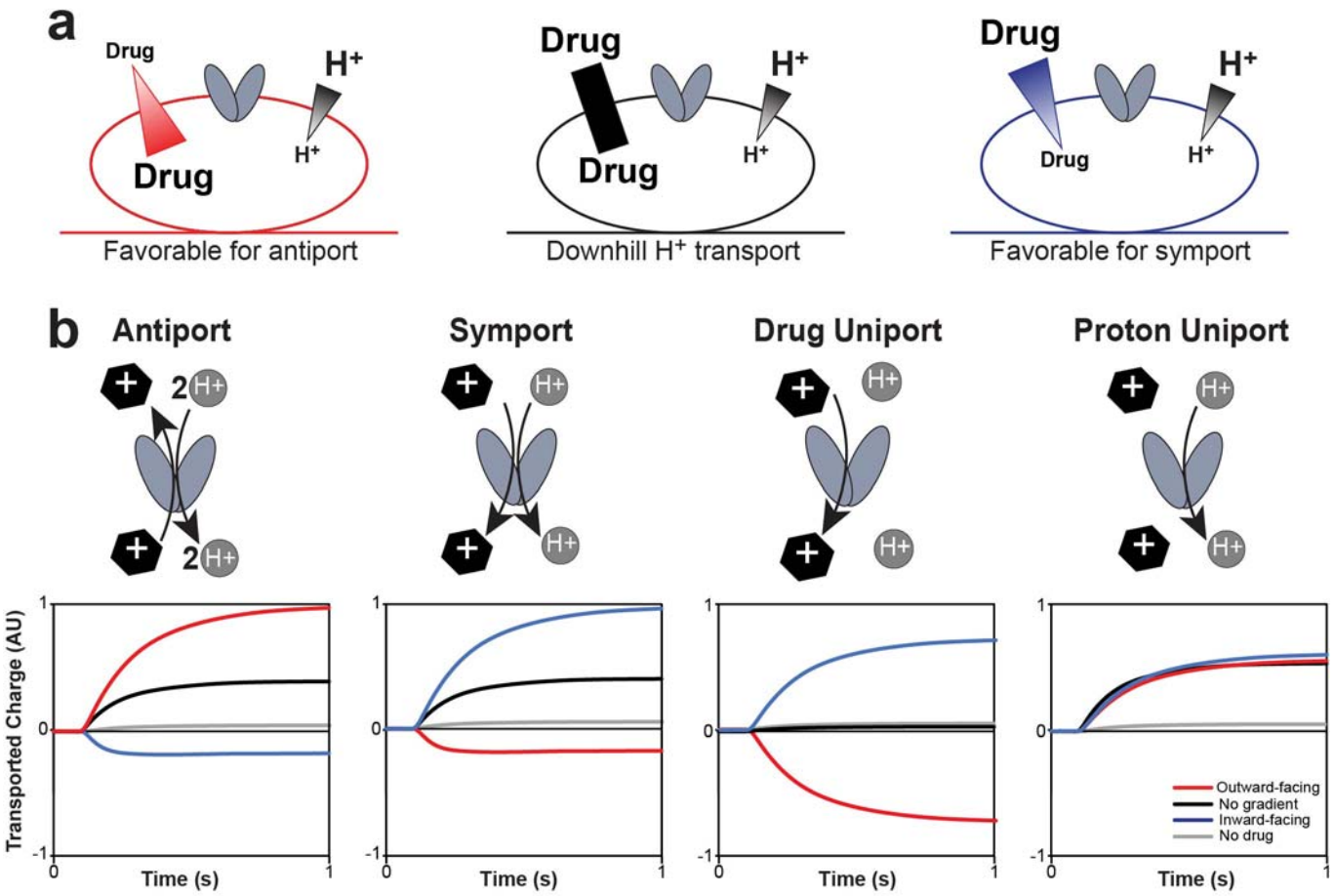

Extended Data Figure 3: Determination of transport mode *in vitro* using solid-supported membrane electrophysiology (SSME). Solid-supported membrane electrophysiology (SSME) allows the measurement of transport currents in proteoliposomes adsorbed onto a sensor, with positive currents indicating charge movement into the liposomes. Transport is initiated by buffer perfusion to create substrate gradients across the liposomal membranes. Various combinations of substrate gradients (A) will have different and predictable effects on the transport signal in the case of antiport, symport, drug uniport or proton uniport (B). In the absence of a drug gradient (black), transport is driven by the two-fold inward-facing proton gradient (pH 7.0 outside, pH 7.3 inside), resulting in a positive signal for the canonical 2 H^+/1 $drug^+$ antiport (net +1 inward per transport cycle), symport (net +1 or +2 inward, for H+ and a neutral or +1 drug), or proton uniport (net +1 inward). For drug uniport, a proton gradient alone will not drive transport. In the case of drug/proton antiport, addition of a much larger (16-fold) drug gradient opposite the proton gradient (red), this will favor antiport and cause a larger positive signal, while aligning the drug- and proton- gradients in the same direction (blue), requires one substrate to move against its concentration gradient. Under our experimental conditions, the driving force from drug gradient "wins" the competition reverses the direction of net transport compared to the 2-fold proton gradient alone. Charge reversal is a hallmark of coupled transport, and the difference between antiport and symport is simply which orientation of the drug gradient enhances proton-driven transport and which orientation reverses net transport. In contrast, uncoupled transport depends solely on the gradient of the uniported substrate. Drug uniport depends only on the direction of the imposed drug gradient and net charge on the drug (shown for a +1 drug, no current would be observed under any condition for an uncharged substrate such as harmane). Proton uniport will result in a consistent, positive signal due to proton flux down the uniform two-fold proton gradient under all three conditions. Transport should be minimal in the absence of drug (gray) if EmrE does not spontaneously leak protons.

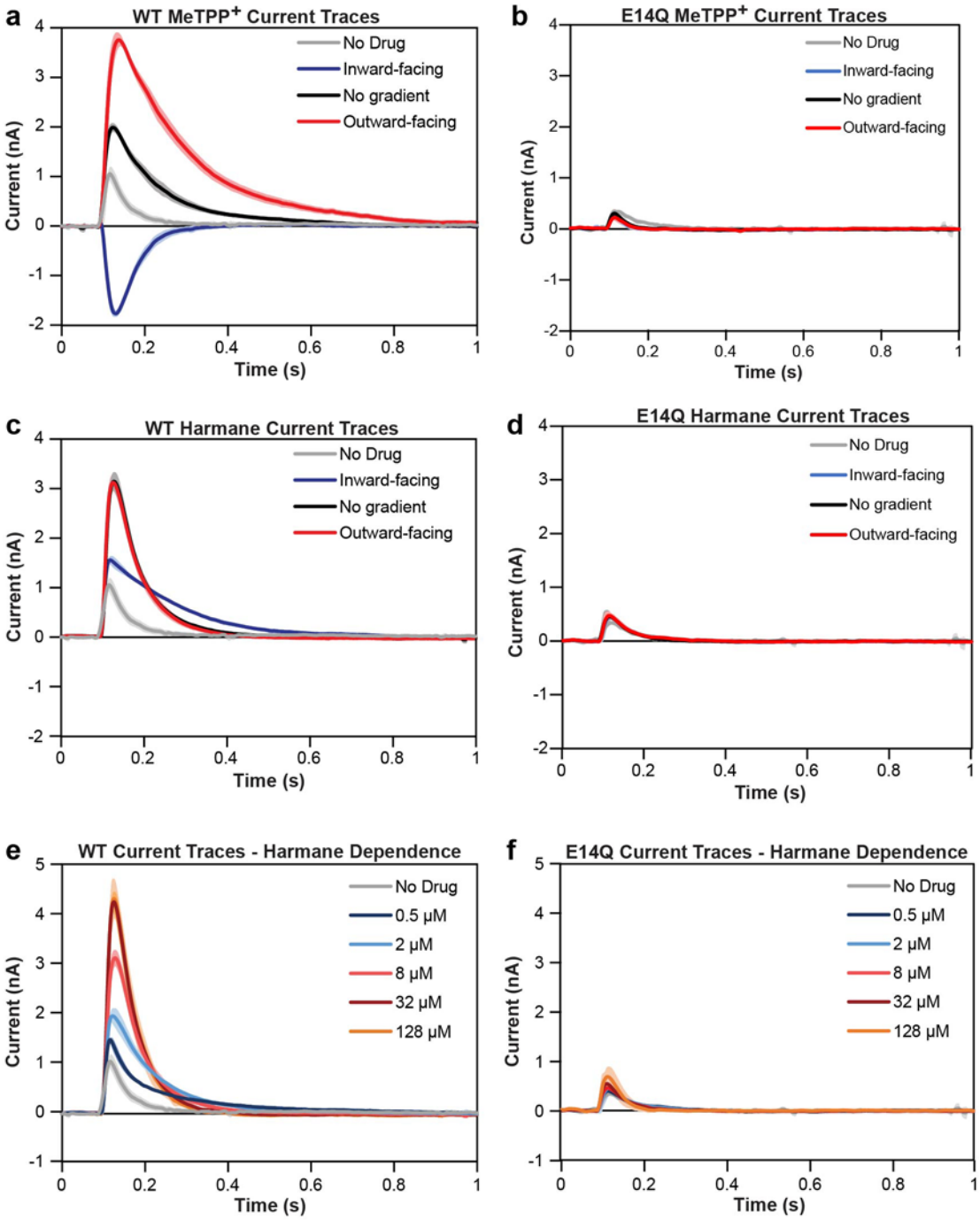

Extended Data Figure 4: Raw current traces for SSME data. Data shown is an average of at least three replicates, with standard deviation indicated by the shaded region. (A) Cartoon scheme of gradient directions for panels (B-E). With both substrates, minimal current is observed for sensors prepared using the non-functional mutant E14Q-EmrE (D, E, and G). $MeTPP^+$ (B and D) behaves as expected for an antiported substrate, with increased signal when the drug and proton gradients are oriented in opposite directions and a reversal of transport direction when the large $MeTPP^+$ gradient is oriented in the same direction as the smaller proton gradient. Harmane (C and E) increases the transport signal compared to a background without drug. The signal is in the direction of downhill proton transport, regardless of the direction of the harmane gradient. (F) Peak current of downhill proton transport increases with increased harmane concentration.

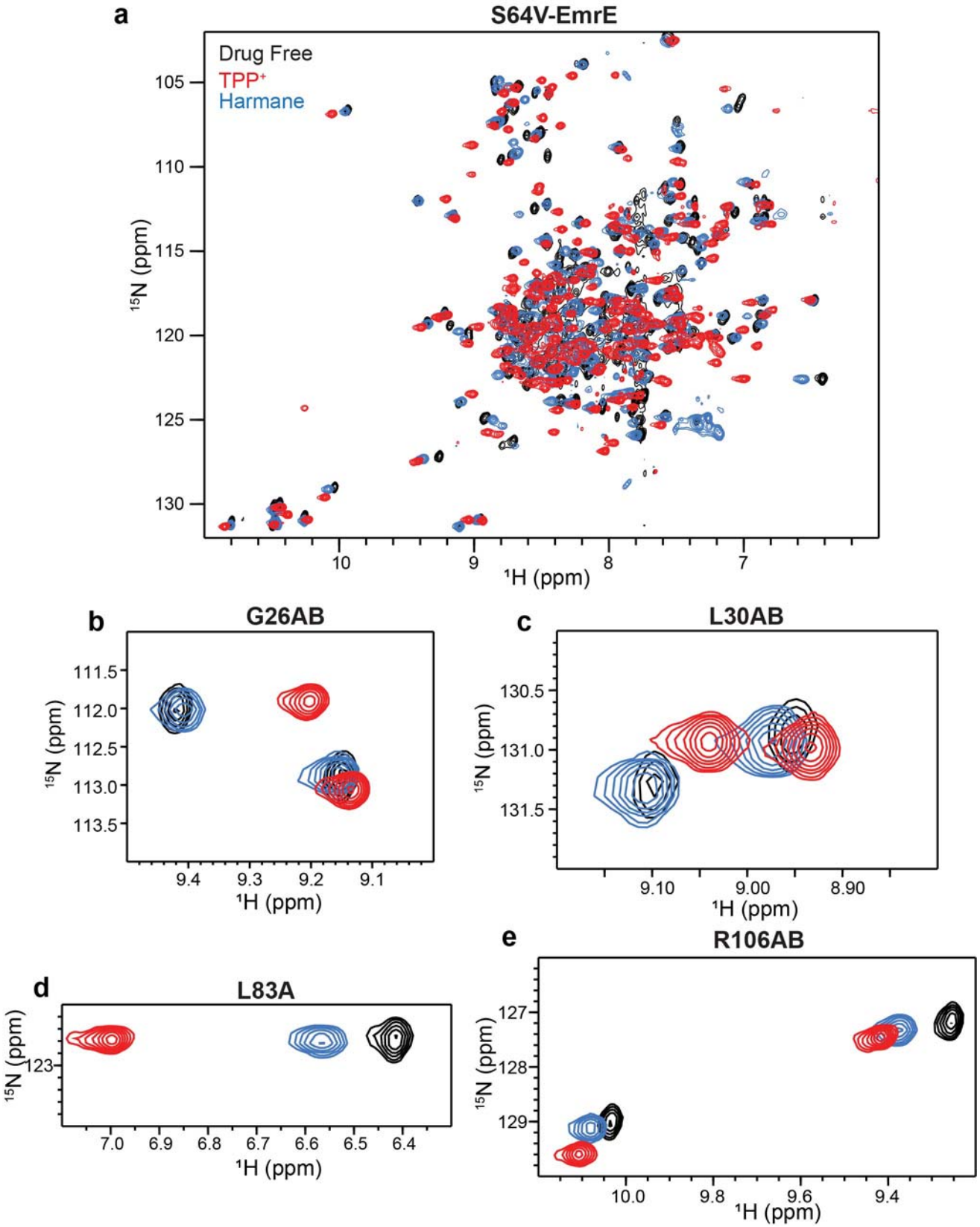

Extended Data Figure 5: NMR spectra of S64V-EmrE upon ligand binding show broad chemical shift perturbations. To monitor the chemical shift perturbation observed for 1 mM S64V-EmrE in isotropic bicelles (q=0.33) using solution NMR ^{1}H-^{15}N TROSY-HSQC spectra acquired at 45 °C, pH 5.8 on a 750MHz Bruker Avance III spectrometer. Spectra of drug free (black) or saturated with harmane (blue) or TPP^{+} (red) are shown with insets (B-E) highlighting the variety of CSPs that occur in the various binding states of EmrE.

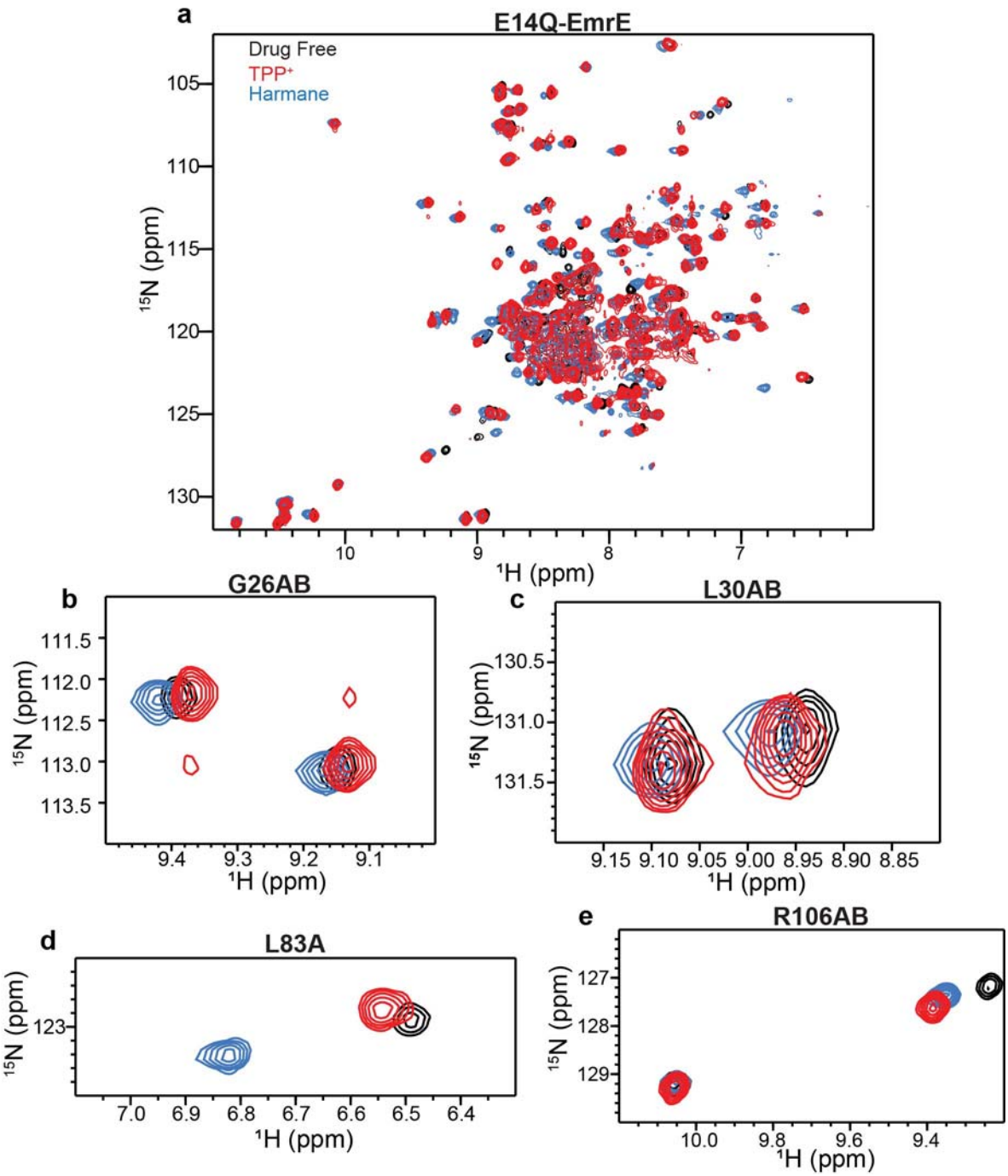

Extended Data Figure 6: NMR spectra of E14Q-EmrE upon ligand binding also show broad chemical shift perturbations. The same experimental approach was used as in Extended Data Figure 5, but with E14Q-EmrE instead of S64V-EmrE. Spectra of drug free (black) or saturated with harmane (blue) or TPP^+ (red) show fewer CSPs when the primary binding site at glutamate 14 is knocked out, but significant CSPs remain for some residues in the spectrum.

Extended Data Table 1: List of Biolog hits displaying resistance or susceptibility phenotypes.

Compound	Hit score*	Formal Charge	Notes
Harmane	-6	0	Reversible inhibitor of monoamine oxidase
Hexachlorophene	-6	0	Antifungal, antiseptic
Menadione	-5	0	Vitamin K
18-crown-6-ether	-5	0	Metal binding
Cefoperazone	-4	0	Cephalosporin antibiotic
Nitrofurazone	-4	+1	Antibiotic
Oxytetracycline	-4	0	Antibiotic
Cobalt (II) chloride	-4	0	metal
Spectinomycin	-4	0	Antibiotic
Ethionamide	-4	0	Prodrug antibiotic,
Rolitetracycline	-3	0	Antibiotic, protein synthesis inhibition
Geneticin disulfate	-3	0	Antibiotic, protein synthesis inhibition
Ruthenium red	-3	0	Inorganic dye
Antimony (III) chloride	-3	0	Metal for vitamin A detection
Troleandomycin	-3	0	Macrolide antibiotic
Cefoxitin	-3	0	Cefalosporin antibiotic
Coumarin	-3	0	Metabolite
Nickel chloride	-3	0	Metal
Oleandomycin	-3	0	Macrolide antibiotic
Erythromycin	-3	0	Macrolide antibiotic
Dodine	-3	0	Fungicide
Glycine HCl	-3	0	Non-essential amino acid
Spiramycin	-3	0	Macrolide antibiotic
Manganese (II) chloride	3	0	Metal
Methyltrioctylammonium chloride	3	+1	Phase transfer catalyst
FCCP	3	0	Proton ionophore
Tetrazolium violet	3	+1	Apoptosis inducer, antineoplastic agent
Cetylpyridinium chloride	4	+1	Antiseptic
Acriflavine	4	+1	Local antiseptic, biological stain
Sanguinarine chloride	4	+1	Toxic polycyclic ammonium ion
Proflavine	4	0	Bacteriostat
Chelerythrine chloride	5	+1	Antibiotic, apoptosis induction
Crystal violet	6	+1	Topical antibiotic
Methyl viologen	8	+2	Desiccant, photosystem-I inhibitor

*Any score ≥ 3 is considered a resistance hit. Any score ≤ -3 is considered a susceptibility hit.

Extended Data Table 2: Buffer conditions for solid-supported membrane electrophysiology experiments.

Drug Gradient	Internal Buffer	External Buffer
Inward-facing	0.5 µM drug 50 nM H^+ (pH 7.3)	8 µM drug 100 nM H^+ (pH 7.0)
Outward-facing	8 µM drug 50 nM H^+ (pH 7.3)	0.5 µM drug 100 nM H^+ (pH 7.0)
No gradient	8 µM drug 50 nM H^+ (pH 7.3)	8 µM drug 100 nM H^+ (pH 7.0)
No drug	50 nM H^+ (pH 7.3)	100 nM H^+ (pH 7.0)